Letter

High sensitivity characterization of an ultrahigh purity NaI(Tl) crystal scintillator with the SABRE proof-of-principle detector

F. Calaprice,[1] S. Copello,[2] I. Dafinei,[3] D. D'Angelo,[4,5] G. D'Imperio,[3] G. Di Carlo,[6] M. Diemoz,[3] A. Di Giacinto,[6] A. Di Ludovico,[1] A. Ianni,[6] M. Iannone,[3] F. Marchegiani,[6] A. Mariani,[7,*] S. Milana,[3] S. Nisi,[6] F. Nuti,[8] D. Orlandi,[6] V. Pettinacci,[3] L. Pietrofaccia,[1] S. Rahatlou,[3,9] M. Souza,[1] B. Suerfu,[10,†] C. Tomei,[3] C. Vignoli,[6] M. Wada,[11] and A. Zani[4]

[1]*Physics Department, Princeton University, Princeton, New Jersey 08544, USA*
[2]*Dipartimento di Fisica, Università degli Studi di Genova and INFN Genova, Genova I-16146, Italy*
[3]*INFN—Sezione di Roma, Roma I-00185, Italy*
[4]*INFN—Sezione di Milano, Milano I-20133, Italy*
[5]*Dipartimento di Fisica, Università degli Studi di Milano, Milano I-20133, Italy*
[6]*INFN—Laboratori Nazionali del Gran Sasso, Assergi (L'Aquila) I-67100, Italy*
[7]*Gran Sasso Science Institute, L'Aquila I-67100, Italy*
[8]*School of Physics, The University of Melbourne, Melbourne, Victoria 3010, Australia*
[9]*Dipartimento di Fisica, Sapienza Università di Roma, Roma I-00185, Italy*
[10]*University of California Berkeley, Department of Physics, Berkeley, California 94720, USA*
[11]*AstroCeNT, Nicolaus Copernicus Astronomical Center of the Polish Academy of Sciences, Warsaw, Poland*

(Received 19 May 2021; accepted 15 June 2021; published 9 July 2021)

We present new results on the radiopurity of a 3.4-kg NaI(Tl) crystal scintillator operated in the SABRE proof-of-principle detector setup. The amount of potassium contamination, determined by the direct counting of radioactive ^{40}K, is found to be 2.2 ± 1.5 ppb, lowest ever achieved for NaI(Tl) crystals. With the active veto, the average background rate in the crystal in the 1–6 keV energy region of interest (ROI) is 1.20 ± 0.05 counts/day/kg/keV, which is a breakthrough since the DAMA/LIBRA experiment. Our background model indicates that the rate is dominated by ^{210}Pb and that about half of this contamination is located in the polytetrafluoroethylene reflector. We discuss ongoing developments of the crystal manufacture aimed at the further reduction of the background, including data from purification by zone refining. A projected background rate lower than ~0.2 counts/day/kg/keV in the ROI is within reach. These results represent a benchmark for the development of next-generation NaI(Tl) detector arrays for the direct detection of dark matter particles.

DOI: 10.1103/PhysRevD.104.L021302

The existence of dark matter is widely accepted [1], yet the particle nature of dark matter is still an open fundamental question. Over the last 25 years, a series of experimental efforts have been made to search for the interaction of dark matter particles with ordinary matter in underground laboratories [1]. However, almost all efforts yielded null results despite the impressive progress in background reduction techniques and detector technologies [2–9]. Experimental efforts have mainly focused on the search for the so-called weakly-interacting massive particles (WIMPs) introduced in 1985 [10]. At present, the best sensitivity has been obtained with a ton-scale liquid xenon time projection chamber: the spin-independent WIMP-nucleon scattering cross section is estimated to be less than $\sim 4 \times 10^{-47}$ cm^2 for a 30-GeV WIMP [2].

As an alternative way to probe particle dark matter, it was shown that the motion of the Earth around the Sun in the dark matter halo can induce an annual modulation in the dark matter interaction rate [11]. The modulation, which is of the order of a few percent in amplitude, has a specific phase that allows to discriminate against other nonmodulating and modulating backgrounds. This approach has been exploited by the DAMA experiment (short for DAMA/NaI and DAMA/LIBRA) [12], which has been observing a clear annual modulation in its array of 250-kg extremely radiopure NaI(Tl) crystals. The annual modulation is consistent with the dark matter hypothesis, but in the standard WIMP framework, it is in tension with other more sensitive direct detection experiments [2–4,6,8,13]. Due to a potential target dependence of WIMP-nucleon interactions, a verification using the same target material is indispensable.

To test the DAMA annual modulation, ANAIS [14] and COSINE [15] are currently operating 112.5 and 106 kg of

*ambra.mariani@gssi.it
†suerfu@alumni.princeton.edu

NaI(Tl) crystal scintillators, respectively. However, they could not provide a definite answer to the long-standing controversy due to their signal-to-noise ratio diminished by constant radioactive backgrounds several times higher than that observed in the DAMA crystals [16,17]. Large fractions of the backgrounds come from radioactive contaminants in the crystal, most notably ^{40}K, ^{210}Pb, and ^{3}H. As a result, current experiments have to run for many years to obtain the required sensitivity [18]. This also indicates that next-generation experiments using NaI(Tl) crystals with radiopurity similar to or below the DAMA level, such as the proposed SABRE experiment [19], can test the annual modulation claim efficiently in a shorter period of time.

In this paper, we report a detailed study of the background components of an ultrahigh radiopurity crystal grown for the SABRE experiment. While preliminary measurements on the same crystal had been performed on the surface [20] and underground inside a passive shielding [21], this study was carried out underground in the SABRE proof-of-principle (PoP) liquid scintillator active veto shielding (Fig. 1) in the Hall C of Laboratori Nazionali del Gran Sasso, Italy [19].

This crystal—NaI-33—was grown using ultrahigh purity NaI powder after a series of R&D activities [22,23]. The preparation of the powder and the crucible were carried out at Princeton [20,23] and the crystal growth was done at Radiation Monitoring Devices in Massachusetts using the vertical Bridgman method [20,24]. The crystal has a mass of 3.4 kg and is wrapped with ten layers of polytetrafluoroethylene (PTFE) tape (about 1 mm) and optically coupled directly to 3-in Hamamatsu R11065 photomultiplier tubes (PMTs) that feature high quantum efficiency and low radioactivity [20]. The crystal-PMT assembly is sealed inside a 2-mm-thick, high-purity copper enclosure [21], whose inner volume is constantly flushed with nitrogen gas to purge moisture and radon. The enclosure is deployed vertically via a 2-mm-thick, 121-cm-long blind-end copper tube into a 1.3-m-diameter, 1.5-m-long stainless steel veto vessel [19]. The veto vessel is filled with 2 tonnes of pseudocumene liquid scintillator and 2.86 g/L of 2,5-diphenyloxazole wavelength shifter, and is instrumented with ten Hamamatsu R5912 8-in PMTs to serve as active veto to enhance background rejection [22,23]. The inner surface of the veto vessel is lined with reflective Lumirror foils to improve light collection [23]. The light yield of the active veto is measured to be 0.52 ± 0.01 photoelectrons/keV (phe/keV) at 2615 keV using a ^{228}Th calibration source. The veto vessel is further shielded from the cavern by an inner high-density polyethylene (HDPE) (10 cm on the top and bottom and at least 40 cm on the sides) and an outer gamma shielding (~90 cm of water on the sides and top and 15 cm of lead on the bottom) [19]. A PTFE tube is used to position wire-mount calibration sources next to the copper enclosure.

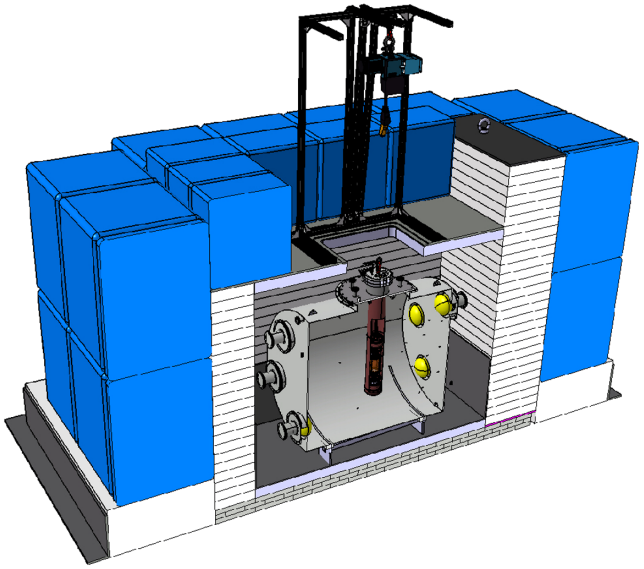

FIG. 1. A CAD rendering of the SABRE PoP detector system with cross sectional view. The detector sits within a catch basin (dark gray) for liquid scintillator. The detector is further shielded by HDPE (white) and either water tanks (blue on the top and sides) or lead (light gray at the bottom). A crane structure mounted at the top is used to place the detector module into the veto vessel.

The data acquisition (DAQ) system consists of a CAEN V1495 custom field-programmable gate array trigger and two CAEN V1720 analog-to-digital converter boards (12-bit resolution, 250 MS/s sampling rate) [23]. The data acquisition is triggered by the logical AND between the two PMTs coupled to the crystal with a 125-ns coincidence window irrespective of the status of the veto detector [23]. Upon trigger, waveforms in the subsequent 3.5-μs window in all PMTs are digitized and read out by a dedicated DAQ software [25].

The light yield and FWHM resolution of NaI-33 crystal scintillator, measured by fitting the 59.5-keV photopeak of an ^{241}Am source, are determined to be 12.1 ± 0.2 phe/keV and 13.5%, respectively. The light yield is slightly higher than that measured in [21]. To determine the background rate in the 1–6 keV region of interest (ROI), data were taken between August 9, 2020 and September 5, 2020 for a total exposure of 26.4 days. To reject coincident backgrounds, events with energy larger than 50 keV in the veto are rejected with 42% veto rejection power in the ROI. In addition, to reduce noise, the following selection criteria (cuts) were applied:

Cut 1 Trigger time delay $\in [-36, 36]$ ns,
Cut 2 No. of clusters in each PMT ≥ 2,
Cut 3 $\langle t \rangle_{600} = \frac{\sum_{t_i<600\text{ ns}} h_i t_i}{\sum_{t_i<600\text{ ns}} h_i} \in [140, 270]$ ns,
Cut 4 $C_{(0,1000)}/h_{\max} > 50$ ns,
Cut 5 $0.2 < C_{(200,400)}/C_{(0,200)} < 0.9$,
Cut 6 $0.1 < C_{(400,600)}/C_{(200,400)} < 0.9$,

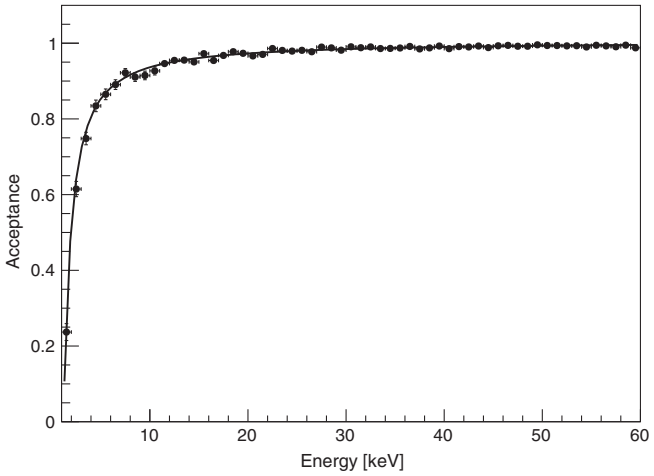

FIG. 2. Acceptance of crystal events after noise rejection cuts as a function of energy, evaluated using a ^{228}Th calibration source. Currently, the acceptance at low energy and henceforth the threshold is mainly limited by the presence of PMT noise. In the future, this will be addressed with better noise-rejecting algorithms and optimized PMT operating voltages and preamplifiers.

where h_i is the amplitude at time t_i in ns, and $C_{(t_i,t_j)}$ is the pulse area between t_i and t_j in ns. Cut 1 imposes a narrower coincidence window between the two pulses in the PMTs. The cluster in Cut 2 is defined as a pulse with amplitude above about one photoelectron, and this cut is used to reject single photoelectron noise. Cuts 3–6 aim at selecting pulselike waveform by imposing constraints on the shape of the waveform: Cut 3 and Cut 4 require the amplitude-weighed mean time and the total area over maximum amplitude to be within a certain range, while Cut 5 and Cut 6 impose constraints on the ratios of pulse areas at different times. These variables are further described in detail in [21]. Figure 2 shows the final acceptance rate as a function of energy after these cuts. The average event acceptance in the ROI is estimated to be 77.6% [26]. The energy spectrum after cuts and efficiency correction is shown in Fig. 3 (black dots) up to 100 keV and in Fig. 4 up to 20 keV. The measured rate in 1–6 keV (1–10 keV) is 1.20 ± 0.05 cpd/kg/keV (1.09 ± 0.04 cpd/kg/keV).

A spectral analysis was performed to quantify the contribution of different background components [26]. Predicted spectral shapes from different background sources were calculated by Monte Carlo [27]. In the fit, the activities of the following components were treated as free or semifree parameters: ^{40}K, ^{210}Pb, ^{3}H, ^{226}Ra, ^{232}Th, ^{129}I, ^{121m}Te, ^{127m}Te, and a flat component which includes ^{87}Rb and other internal and external background contributions. In addition, ^{210}Pb from the PTFE reflector wrapping the crystal was included to reproduce the peak at ~12 keV due to x-rays from ^{210}Pb. In the spectral fit, a Gaussian penalty was applied to ^{40}K with mean equal to 0.14 ± 0.01 mBq/kg corresponding to the prediction from inductively coupled plasma mass spectrometry measurements [20]. Assuming secular equilibrium for ^{226}Ra and ^{232}Th chain segments, Gaussian penalties [(5.9 ± 0.6) μBq/kg for ^{226}Ra and (1.6 ± 0.3) μBq/kg for ^{232}Th] were implemented based on measurements from ^{214}Bi-Po and ^{212}Bi-Po time-correlated events, respectively [21].

The result of the fit is shown in Figs. 3 and 4. The p-value of the fit is equal to 0.26 with $\chi^2/N_{\mathrm{d.o.f.}} = 96/88$. Table I summarizes the breakdown of the background components determined from the fit. The background rate in the ROI, dominated by ^{210}Pb in the bulk of the crystal and on the surface of the PTFE reflector, is found to be conservatively equal to 1.16 ± 0.10 cpd/kg/keV. The ^{40}K activity is estimated to be 0.14 ± 0.01 mBq/kg. This value is consistent with an independent measurement of ^{40}K using the coincidence between 3.2-keV X-ray/auger electrons in the

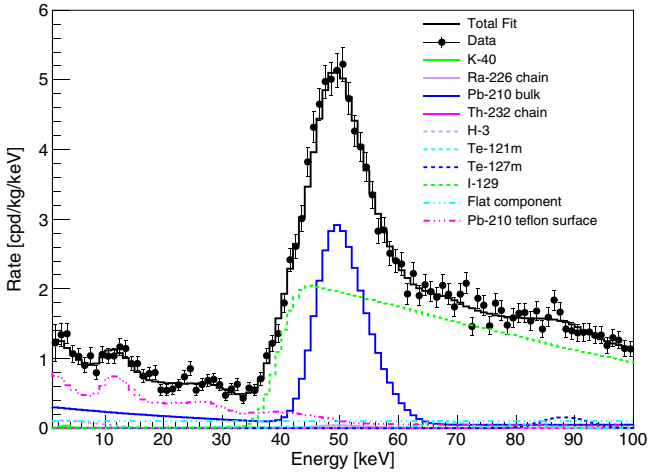

FIG. 3. Energy spectrum from NaI-33 up to 100 keV with a spectral fit. The spectrum is shown after selection cuts and efficiency correction.

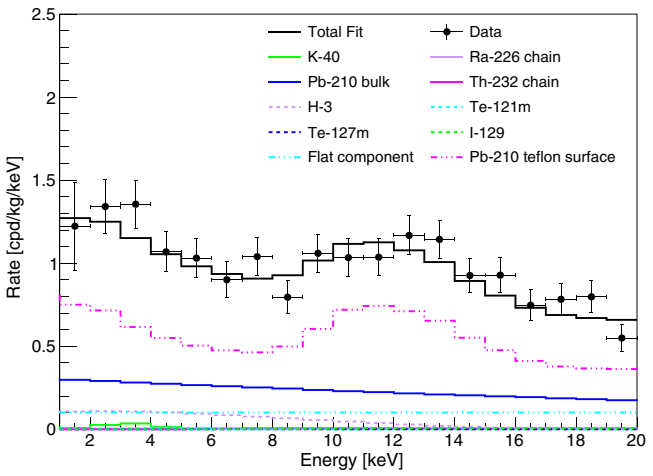

FIG. 4. Energy spectrum from NaI-33 below 20 keV with the spectral fit. The spectrum is shown after selection cuts and efficiency corrected.

TABLE I. Background components in NaI-33 from the spectral fit, current rate in ROI (1–6 keV), and projected rate in ROI for future crystals. The future rate assumes underground crystal production with zone-refining purification and improved reflector radiopurity. The activity of ^{210}Pb in the reflector is normalized to the crystal mass for comparison with bulk activities. Upper limits are given as one-sided 90% C.L. Rates are conservatively calculated using upper limits.

Source	Activity in NaI-33 (mBq/kg)	Rate in ROI in NaI-33 (cpd/kg/keV)	Projected rate in ROI (cpd/kg/keV)
^{40}K	0.14 ± 0.01	0.018 ± 0.001	≤ 0.004
^{210}Pb (bulk)	0.41 ± 0.02	0.28 ± 0.01	$\leq 0.093 \pm 0.003$
^{226}Ra	0.0059 ± 0.0006	0.0044 ± 0.0005	0.0044 ± 0.0005
^{232}Th	0.0016 ± 0.0003		
^{3}H	0.012 ± 0.007	≤ 0.12	…
^{129}I	1.34 ± 0.04		
^{121m}Te	≤ 0.084	≤ 0.011	…
^{127m}Te	0.016 ± 0.006		
^{210}Pb (PTFE)	0.32 ± 0.06	0.63 ± 0.09	≤ 0.007
Other		0.10 ± 0.05	0.10 ± 0.05
Total		1.16 ± 0.10	0.21 ± 0.05

crystal and 1.46 MeV gamma ray in the active veto, which yielded 0.07 ± 0.05 mBq/kg (2.2 ± 1.5 ppb, or < 4.7 ppb at 90% C.L.) despite limited statistics.

The activity of bulk ^{210}Pb is determined to be 0.41 ± 0.02 mBq/kg, consistent with earlier measurements using α counting of ^{210}Po [20,21]. Although this value is about 1 order of magnitude larger than that in DAMA, it is smaller than those in ANAIS and COSINE, where on average the activity is about 1 mBq/kg [14,28].

The activity of ^{210}Pb in the reflector is measured to be 1.1 ± 0.2 mBq, with the first 4 μm from the crystal surface mostly responsible for background events. Although the commercial PTFE tape was carefully cleaned by acid leach [23], this analysis indicates that the cleaning procedure is not very effective in removing ^{210}Pb impurities. The ^{210}Pb radioactivity of PTFE has been studied by other experiments: the special PTFE used in the CUORE-0 experiment has a ^{210}Pb activity ≤ 123 μBq/kg$_{\mathrm{PTFE}}$ (90% C.L.) [29,30]; in the DarkSide-50 experiment [31], ^{210}Pb activity in PTFE is measured to be ≤ 38 mBq/kg$_{\mathrm{PTFE}}$ (90% C.L.) by γ-spectroscopy [32] and ≤ 46 mBq/kg$_{\mathrm{PTFE}}$ by ^{210}Po α counting [33]. These considerations imply that the background due to the PTFE reflector can be reduced to a secondary component by custom or special manufacturing of the PTFE tapes.

The activation rate of ^{3}H in NaI is measured to be 83 ± 27 cpd/kg by ANAIS [34]. NaI-33 has undergone a 9-month surface exposure at sea level and a 12-month cooling underground. At the predicted activation rate, NaI-33 would have seen a ^{3}H activity of (37 ± 12) μBq/kg. The actual ^{3}H activity is estimated to be (12 ± 7) μBq/kg. Although limited by statistics, the ^{3}H production rate in NaI-33 seems to be lower. One possibility is that the previously reported ^{3}H rate is not entirely due to cosmogenic ^{3}H, and instead varying amount of ^{3}H is introduced into the crystal as NaOH impurity depending on the powder drying and crystal growth method [23].

To further improve radiopurity of crystals to be grown in the future, we have tested the zone refining of ultrahigh purity NaI powder. Table II, reproduced from [35], shows that many impurities are greatly reduced in the first three samples (about 50% of the ingot), and in particular ^{40}K and ^{87}Rb are reduced to negligible levels.

Quantitatively, the reduction of K and Rb depends on the segregation coefficient k and the fraction of the purified material to be reserved [23,35]. The segregation coefficient of K is estimated to be 0.57, while for Rb it is < 0.59 at 90% C.L. [35]. Table III lists the reduction of impurity concentration for different combinations of number of zone passes and fraction of the material reserved (Fig. 9 in [35]). Based on this, the purity can be further improved by a factor of 10 with 25 zone passes (1-week processing time) and at the cost of 20% of the initial material, or at the same cost of

TABLE II. In the zone-refining test, 53 zone passes were performed on 744 g of ultrahigh purity NaI powder, and five samples were taken from different ingot locations and analyzed to determine the purification efficiency [35]. A few other elements are included to show effectiveness for other metallic impurities.

Isotope	Impurity concentration (ppb)					
	Powder	S_1	S_2	S_3	S_4	S_5
^{39}K	7.5	< 0.8	< 0.8	1	16	460
^{85}Rb	< 0.2	< 0.2	< 0.2	< 0.2	< 0.2	0.7
^{208}Pb	1.0	0.4	0.4	< 0.4	0.5	0.5
^{24}Mg	14	10	8	6	7	140
^{133}Cs	44	0.3	0.2	0.5	3.3	760
^{138}Ba	9	0.1	0.2	1.4	19	330

TABLE III. Reduction of K for different numbers of passes and when different fractions of the ingot are reserved.

No. of passes	Impurity reduction				
	Fraction of material retained				
	50%	60%	70%	80%	90%
10	0.3	0.36	0.42	0.48	0.56
25	0.03	0.050	0.07	0.11	0.25
50	0.001	0.0026	0.0086	0.037	0.18

material but with 50 zone passes (2-week processing time), the average purity can be improved by a factor of 25. Therefore, for future NaI crystals, the background due to ^{40}K and ^{87}Rb can be made subdominant compared to the amplitude of the modulation.

Pb is more or less uniformly reduced by a factor of ≈3 without following the typical impurity distribution of zone refining [35]. Although one can still exploit this factor of 3, zone refining is not as efficient in removing ^{210}Pb. Thus, we have started new R&D activity to explore alternative purification methods and have achieved preliminary progress. Since the analysis of data on the removal of Pb is still in progress, in this paper, we adopt the conservative reduction factor for ^{210}Pb obtained from zone refining alone.

With the aforementioned measures, a projected background rate of 0.21 cpd/kg/keV can be practically achieved in the future SABRE crystals (see Table I). In this projection, we have assumed the contamination level of NaI-33 for ^{40}K and bulk ^{210}Pb scaled by the reduction factor of zone refining in Table III. For ^{210}Pb in the reflector, we have assumed a contamination equal to the upper limit for the PTFE measured in DarkSide-50. To suppress cosmogenic backgrounds to a negligible level, we are also investigating the possibility of establishing an underground crystal growth facility at the Canfranc Laboratory in Spain [36].

To quantify the sensitivity to the dark matter–induced annual modulation, the figure-of-merit (FoM) defined in [37] can be used where a small FoM indicates a high sensitivity. In this framework, the DAMA/LIBRA phase II [38] has FoM $= 8 \times 10^{-4}$ d^{-1} kg^{-1} keV^{-1}. A similar value of FoM can be obtained with a 60 kg × 5 yr exposure and the predicted background rate of 0.21 cpd/kg/keV in Table I. With the same exposure and background rate, the minimum detectable rate [39] is expected to be $\leq (2 \pm 1) \times 10^{-3}$ cpd/kg/keV at 90% C.L., which is about 5 times less than DAMA modulation amplitude of $10.5 \pm 1.1 \times 10^{-3}$ cpd/kg/keV in 1–6 keV ROI [38]. On the other hand, for the current generation of NaI(Tl) detector arrays, several decades are needed to obtain the same FoM as DAMA/LIBRA phase II. Therefore, the present results obtained from NaI-33 together with the planned improvements discussed above will be fundamental for the next-generation NaI-based dark matter detectors.

The growth of NaI-33 and its characterization in the SABRE detector are a breakthrough in the technology to support next-generation NaI experiments to probe the long-standing DAMA result: the background rate in the 1–6 keV ROI is determined to be 1.20 ± 0.05 cpd/kg/keV, several times lower than all presently running NaI-based experiments except DAMA. At present, the dominant backgrounds are due to bulk ^{210}Pb and ^{210}Pb in the PTFE reflector. With a combination of zone refining, special low-radioactivity PTFE tape, and underground growth of crystals, the background in the ROI in future crystals can be further reduced to ≤ 0.21 cpd/kV/keV. This result marks a significant improvement in the quest for testing the dark matter–induced annual modulation and paves the road to the next-generation NaI-based experiments with higher sensitivities.

ACKNOWLEDGMENTS

This work was supported by INFN funding and National Science Foundation under the Awards No. PHY-1242625, No. PHY-1506397, and No. PHY-1620085. We thank Ezio Previtali, Andrea Giuliani, and Monica Sisti for discussions about PTFE radiopurity in CUORE. We thank Fausto Ortica and Aldo Romani from Perugia University for support in photospectrometric measurements. We thank the Gran Sasso Laboratory for the support during the installation of the SABRE PoP setup.

[1] G. Bertone and D. Hooper, Rev. Mod. Phys. **90**, 045002 (2018).
[2] E. Aprile, J. Aalbers, F. Agostini, M. Alfonsi, L. Althueser, F. Amaro, M. Anthony, F. Arneodo, L. Baudis *et al.*, Phys. Rev. Lett. **121**, 111302 (2018).
[3] D. Akerib, S. Alsum, H. Araújo, X. Bai, A. Bailey, J. Balajthy, P. Beltrame, E. Bernard, A. Bernstein, T. Biesiadzinski *et al.*, Phys. Rev. Lett. **118**, 021303 (2017).
[4] X. Cui, A. Abdukerim, W. Chen, X. Chen, Y. Chen, B. Dong, D. Fang, C. Fu, K. Giboni, F. Giuliani *et al.*, Phys. Rev. Lett. **119**, 181302 (2017).
[5] P. Agnes, I. Albuquerque, T. Alexander, A. Alton, G. Araujo, M. Ave, H. Back, B. Baldin, G. Batignani, K. Biery *et al.*, Phys. Rev. D **98**, 102006 (2018).
[6] G. Angloher, M. Bauer, I. Bavykina, A. Bento, C. Bucci, C. Ciemniak, G. Deuter, F. von Feilitzsch, D. Hauff, P. Huf *et al.*, Eur. Phys. J. C **72**, 1971 (2012).
[7] A. Aguilar-Arevalo, D. Amidei, D. Baxter, G. Cancelo, B. C. Vergara, A. Chavarria, J. DOlivo, J. Estrada, F. Favela-Perez, R. Gaior *et al.*, Phys. Rev. Lett. **125**, 241803 (2020).
[8] R. Agnese, T. Aralis, T. Aramaki, I. Arnquist, E. Azadbakht, W. Baker, S. Banik, D. Barker, D. Bauer, T. Binder *et al.*, Phys. Rev. Lett. **121**, 051301 (2018).

[9] R. Agnese, T. Aralis, T. Aramaki, I. Arnquist, E. Azadbakht, W. Baker, S. Banik, D. Barker, D. Bauer, T. Binder *et al.*, Phys. Rev. Lett. **122**, 069901 (2019).

[10] M. W. Goodman and E. Witten, Phys. Rev. D **31**, 3059 (1985).

[11] A. K. Drukier, K. Freese, and D. N. Spergel, Phys. Rev. D **33**, 3495 (1986).

[12] R. Bernabei *et al.*, Prog. Part. Nucl. Phys. **114**, 103810 (2020).

[13] P. Agnes, I. Albuquerque, T. Alexander, A. Alton, G. Araujo, D. M. Asner, M. Ave, H. O. Back, B. Baldin, G. Batignani *et al.*, Phys. Rev. Lett. **121**, 081307 (2018).

[14] J. Amaré, S. Cebrián, I. Coarasa, C. Cuesta, E. García, M. Martínez, M. Oliván, Y. Ortigoza, A. O. de Solórzano, J. Puimedón *et al.*, Eur. Phys. J. C **79**, 228 (2019).

[15] G. Adhikari, P. Adhikari, E. B. de Souza, N. Carlin, S. Choi, W. Choi, M. Djamal, A. Ezeribe, C. Ha, I. Hahn *et al.*, Eur. Phys. J. C **78**, 107 (2018).

[16] J. Amaré, S. Cebrián, I. Coarasa, C. Cuesta, E. García, M. Martínez, M. Oliván, Y. Ortigoza, A. O. de Solórzano, J. Puimedón *et al.*, Phys. Rev. Lett. **123**, 031301 (2019).

[17] G. Adhikari, P. Adhikari, E. B. de Souza, N. Carlin, S. Choi, M. Djamal, A. Ezeribe, C. Ha, I. Hahn, E. Jeon *et al.*, Phys. Rev. Lett. **123**, 031302 (2019).

[18] J. Amaré, S. Cebrián, D. Cintas, I. Coarasa, E. García, M. Martínez, M. Oliván, Y. Ortigoza, A. O. de Solórzano, J. Puimedón *et al.*, Phys. Rev. D **103**, 102005 (2021).

[19] M. Antonello, E. Barberio, T. Baroncelli, J. Benziger, L. Bignell, I. Bolognino, F. Calaprice, S. Copello, D. Dangelo, G. Dimperio *et al.*, Eur. Phys. J. C **79**, 363 (2019).

[20] B. Suerfu, M. Wada, W. Peloso, M. Souza, F. Calaprice, J. Tower, and G. Ciampi, Phys. Rev. Research **2**, 013223 (2020).

[21] M. Antonello, I. Arnquist, E. Barberio, T. Baroncelli, J. Benziger, L. Bignell, I. Bolognino, F. Calaprice, S. Copello, I. Dafinei *et al.*, Eur. Phys. J. C **81**, 299 (2021).

[22] E. K. Shields, SABRE: A search for dark matter and a test of the DAMA/LIBRA annual-modulation result using thallium-doped sodium-iodide scintillation detectors, Ph.D. thesis, Princeton University, 2015, https://inspirehep.net/literature/1466707.

[23] Suerfu, Developing ultra-low background sodium-iodide crystal detector for dark matter searches, Ph.D. thesis, Princeton University, 2018, https://dataspace.princeton.edu/handle/88435/dsp01df65vb629.

[24] P. W. Bridgman, Proc. Am. Akad. Arts Sci. **60**, 305 (1925).

[25] B. Suerfu, J. Instrum. **13**, T12004 (2018).

[26] A. Mariani, The proof-of-principle of the SABRE experiment for the search of galactic dark matter through annual modulation, Ph.D. thesis, Gran Sasso Science Institute, 2021.

[27] M. Antonello, E. Barberio, T. Baroncelli, J. Benziger, L. Bignell, I. Bolognino, F. Calaprice, S. Copello, D. DAngelo, G. DImperio *et al.*, Astropart. Phys. **106**, 1 (2019).

[28] G. Adhikari, P. Adhikari, E. B. de Souza, N. Carlin, J. Choi, S. Choi, M. Djamal, A. Ezeribe, L. Franca, C. Ha *et al.*, arXiv:2101.11377.

[29] C. Alduino, K. Alfonso, D. Artusa, F. Avignone III, O. Azzolini, M. Balata, T. Banks, G. Bari, J. Beeman, F. Bellini *et al.*, J. Instrum. **11**, P07009 (2016).

[30] C. Alduino, K. Alfonso, D. Artusa, F. Avignone, O. Azzolini, T. Banks, G. Bari, J. Beeman, F. Bellini, A. Bersani *et al.*, Eur. Phys. J. C **77**, 13 (2017).

[31] P. Agnes, T. Alexander, A. Alton, K. Arisaka, H. Back, B. Baldin, K. Biery, G. Bonfini, M. Bossa, A. Brigatti *et al.*, Phys. Lett. B **743**, 456 (2015).

[32] M. Laubenstein and P. Meyer (private communication).

[33] G. Zuzel, K. Pelczar, and M. Wójcik, Appl. Radiat. Isot. **126**, 165 (2017).

[34] J. Amar *et al.*, Astropart. Phys. **97**, 96 (2018).

[35] B. Suerfu, F. Calaprice, and M. Souza, arXiv:2105.06431 [Phys. Rev. Applied (to be published)].

[36] A. Ianni, J. Phys. **675**, 012002 (2016).

[37] I. Coarasa, J. Amaré, S. Cebrián, C. Cuesta, E. García, M. Martínez, M. Oliván, Y. Ortigoza, A. O. de Solórzano, J. Puimedón *et al.*, Eur. Phys. J. C **79**, 233 (2019).

[38] R. Bernabei, P. Belli, A. Bussolotti, F. Cappella, V. Caracciolo, R. Cerulli, C. Dai, A. d'Angelo, A. Di Marco, H. He *et al.*, Nucl. Phys. At. Energy **19**, 307 (2018).

[39] N. Tsoulfanidis, *Measurement and Detection of Radiation* (CRC press, Boca Raton, Florida, 2010).